Met. Mater. Int., Vol. 23, No. 1 (2017), pp. 68~75
doi: 10.1007/s12540-017-6384-7

Evaluation of Dynamic Recrystallization Behaviors in Hot-Extruded AA5083 Through Hot Torsion Tests

Kwang-Tae Son[1], Ji-Woon Lee[1], Taek-Kyun Jung[1], Hyun-Jin Choi[1], Sang-Wook Kim[1], Shae K. Kim[2], Young-Ok Yoon[2], and Soong-Keun Hyun[1,*]

[1]Department of Materials Science and Engineering, Inha University, Incheon 22212, Republic of Korea
[2]Rare Metal R and BD Group, Korea Institute of Industrial Technology (KITECH), Incheon 21999, Republic of Korea

(received date: 2 June 2016 / accepted date: 28 July 2016)

Hot torsion tests were carried out to evaluate the dynamic recrystallization (DRX) behaviors of hot-extruded AA5083 at various deformation conditions. Flow curves showed the peak followed by the flow softening to the steady-state or to the failure strain, indicating that the DRX occurred during deformation. The peak stress increased as the temperature decreased and the strain rate increased. Constitutive relationship and Zener-Hollomon (Z) parameter were used to evaluate the DRX characteristics. Peak and steady-state stresses were generalized by the dimensionless parameter, Z/A, to reveal the DRX mechanism. The empirical relationship of the DRXed grain size with the deformation conditions was established, and decreased with increasing Z parameter. The relationship for the fraction of DRXed grains was established as a function of the effective strain at given deformation conditions from the experimental data. The Avrami relationship based on micro-hardness measurement was used to describe the DRX kinetics, and was fitted well with the observed DRX fraction.

Keywords: alloys, hot working, recrystallization, hot torsion test, optical microscopy

1. INTRODUCTION

Non-heat treatable Al-Mg alloys have been considered as possible structural materials for the use in the shipbuilding industries due to their reasonable strength, excellent corrosion resistance and good weldability [1]. As the mechanical properties are determined during the thermo-mechanical process, the appropriate design of the process schedule is required for the better quality of the products. Especially, the decrease in ductility is a main problem for these alloys, which caused by the work-hardening during the process. It is believed that the development of forming capability will enhance the potential for the various applications [2-4].

During the hot deformation process of Al-Mg alloys, the dynamic recrystallization (DRX) is generally presented as a dynamic softening mechanism [5-7]. DRX behaviors of these alloys have been widely studied, especially for their mechanism and microstructural behavior [5-9]. However, the kinetics of DRX and dynamically recrystallized grain size (D_{DRX}) at a given deformation condition are still insufficient for these alloys. DRX fraction and D_{DRX} are important factors to estimate the mechanical properties of hot-worked materials. In general, the strength of a material increased with decreasing average grain size, and additionally, raise in DRX fraction leads to increase in the fraction of grain boundaries that facilitates grain boundary sliding (GBS) associated with hot workability [7,10]. In addition, these factors could be utilized for the prediction of microstructure at given deformation conditions. As the mechanical properties of a material generally vary with its microstructure, the prediction of microstructure would be helpful for the design of products with desirable properties. In this study, hot torsion test was carried out to investigate DRX characteristics of hot-extruded AA5083 in the view point of microstructure prediction.

2. EXPERIMENTAL PROCEDURES

The hot-extruded AA5083 rods were supplied by Korea Institute of Industrial Technology and had the chemical compositions given in Table 1. The rods with a diameter of 30 mm have been reduced from direct chill cast billets with a diameter of 375 mm by hot extrusion. The rods were machined into torsion specimens, which had a gauge length of 20 mm and a radius of 5 mm, with the axis parallel to the extrusion direction. The tests were carried out with a hot torsion test, which consisted of a gripping zig, a rotating zig, a water

*Corresponding author: skhyun@inha.ac.kr

Table 1. Chemical composition of hot-extruded AA5083

Alloy	Elements (wt%)							
	Al	Mg	Mn	Fe	Cr	Si	Cu	Zn
AA5083	Bal.	4.70	0.76	0.19	0.09	0.08	0.03	0.02

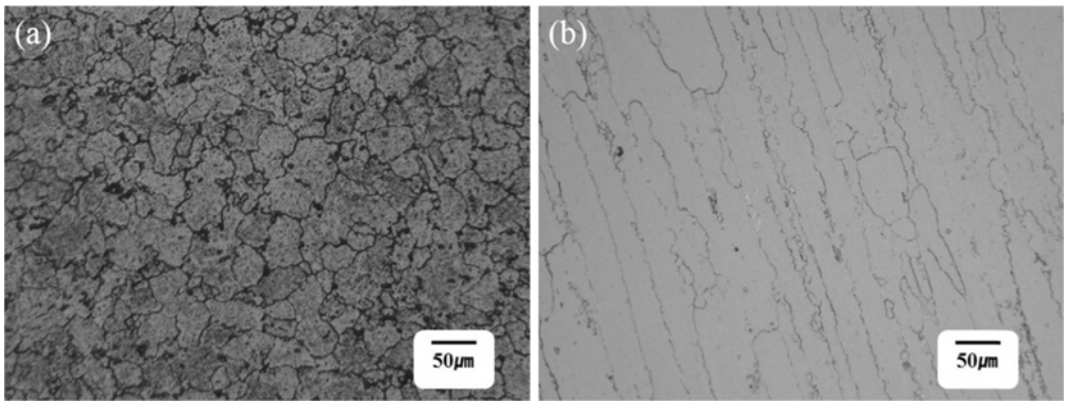

Fig. 1. Optical micrographs for initial microstructure of hot-extruded AA5083 with (a) transverse and (b) longitudinal directions to torsion axis after annealing.

quenching system and an infrared heating furnace providing considerably high heating rate of 1 K/s. The torsion specimens were annealed at 793 K for 1.5 h before conducting the hot torsion tests. The annealed microstructures of aluminum alloy are shown in Fig. 1. The hot torsion tests were carried out with strain rates of 0.05, 0.5 and 5 s^{-1} and at the temperatures of 573, 673 and 773 K, this condition range was referred from previous studies for hot deformation [11,12].

The torsional moment (M) - torsional angle (θ) curves were changed into the effective stress (σ)-effective strain (ε) curves according to the following equations established by Fields and Backofen combined with the von Mises yield criterion [13].

$$\sigma = \frac{\sqrt{3}M(3+p+q)}{2\pi r^3}, \tag{1}$$

$$\varepsilon = \frac{r\theta}{\sqrt{3}L}, \tag{2}$$

where, r and L are a radius and a length of the gauge section in the torsion specimens, respectively. The strain rate sensitivity (p) was calculated from the plots between $\ln M$ and $\ln\dot{\theta}$, and the work hardening rate (q) was given as zero [8,14].

The deformed microstructures of hot-torsioned specimens were observed by optical microscopy (OM). The specimens were cut parallel to the torsional axis at a distance of 0.7 r due to inhomogeneous shear strain along to specimen radius of torsion test [15]. The specimens were prepared by the typical metallographic preparation method, and were etched by 10% H_3PO_4 in distilled water. D_{DRX} and a DRX fraction of the torsion specimens with each experimental condition were estimated through observed microstructure and were digitally calculated using an image analyzing software. Vicker's micro-hardness measurement was conducted, using 0.5-kg load on the central region of polished specimens where maximum deformation was anticipated, to research the DRX fraction property. Zener-Hollomon (Z) parameter was used to describe the DRX behaviors in this study. Z parameter is identical to the following relationship:

$$Z = \dot{\varepsilon}\exp\left(\frac{Q}{RT}\right), \tag{3}$$

where Z, $\dot{\varepsilon}$, Q, R and T are Zener-Hollomon parameter, a strain rate, the activation energy for deformation, the gas constant and the temperature, respectively.

3. RESULTS AND DISCUSSION

3.1. Flow curve analysis

Representative effective stress-effective strain curves for hot-extruded AA5083 conducted at various deformation conditions are presented in Fig. 2. All the curves showed that the flow stresses increased up to a peak strain (ε_p), and decreased as the deformation proceeded. At the highest strain rates, the samples were fractured at earlier strain without showing the steady state at all testing temperatures. On the contrary, the steady state was shown at lower strain rates (0.05 and 0.5 s^{-1}). The failure strain decreased as the strain rate increased at 573 K. However, the failure strains were highest at the strain rate of 0.5 s^{-1} at higher temperature.

The decline of the flow stress is probably due to the dynamic softening such as dynamic recovery (DRV) and DRX that caused by dislocation accumulation and subgrain formation [5,6,9]. These dynamic softening behaviors are derived from

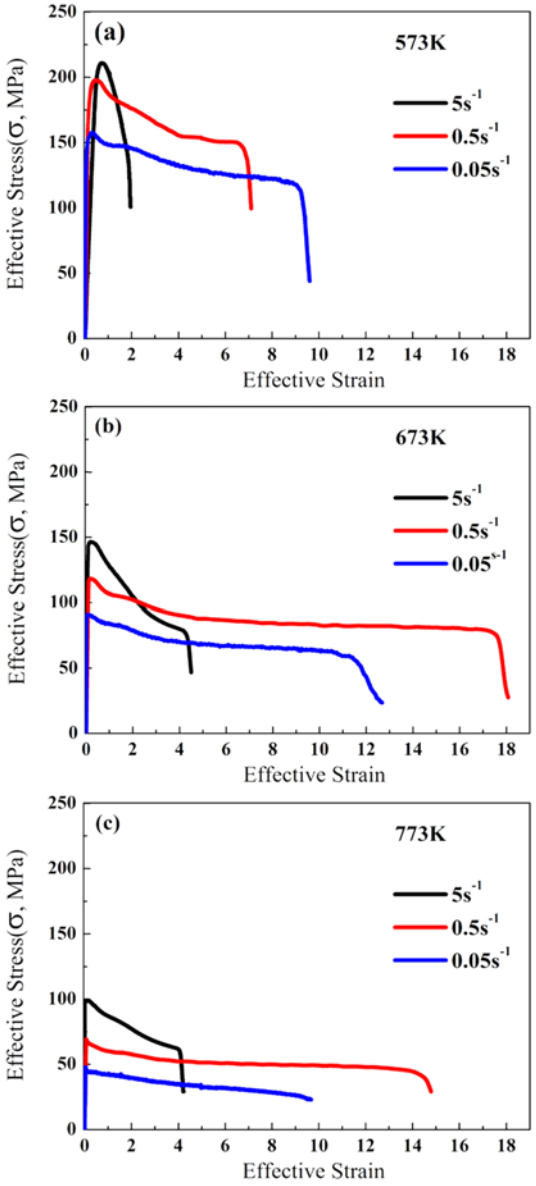

Fig. 2. Effective stress-strain curves of hot-extruded AA5083 obtained from hot torsion test at (a) 573 K, (b) 673 K and (c) 773 K with various strain rates.

stored deformation energy and thermal activation energy of dislocation movement. These phenomena are considerably constrained by the rapid increase of dislocation density within a short interval, in other words, at a higher strain rate. For example, Fig. 2 shows the rise in flow stress with increasing strain rates at a constant temperature, which was caused by suppression of dynamic softening due to relatively large deformation during the same time. As a result, the steady state is observed at only those strain rates of 0.5 and 0.05 s^{-1}, which seems to have several benefits on development of dynamic softening.

From the experimental data, hyperbolic sine function combined with Arrhenius equation was used to determine

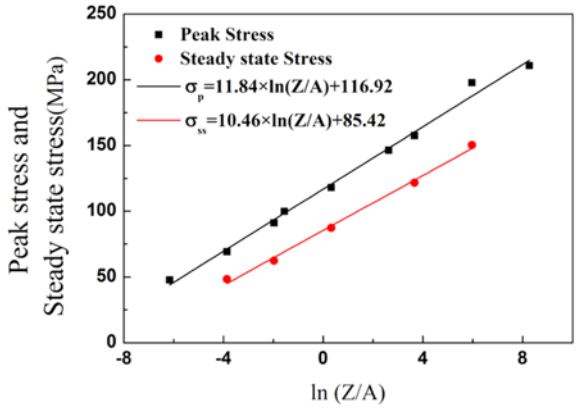

Fig. 3. Relationships between peak and steady state stresses and dimensionless parameter, Z/A for hot-extruded AA5083.

the relationship among peak stress (σ_p), strain rate and temperature on the flow curves as follows:

$$\dot{\varepsilon} = 4.02 \times 10^{13} \{\sinh(0.007\sigma_p)^{7.64}\} \exp\left(-\frac{181.62}{RT}\right), \quad (4)$$

This equation describes the behavior of the materials deformed at different temperatures and strain rates. It is useful to predict the deformation resistance for given deformation conditions.

The dependence of the peak and steady-stress stresses (σ_{ss}) on temperature and strain rate for the tested alloy can be expressed by the following equations with dimensionless parameter Z/A [16]:

$$\sigma_p = 11.84 \times \ln(Z/A) + 116.92\,, \quad (5)$$

$$\sigma_{ss} = 10.46 \times \ln(Z/A) + 85.42\,, \quad (6)$$

where A is a constant of the constitutive equation, and the value is equal to 4.02×10^{13} as presented in Eq. (4). The slope of Eqs. (5) and (6) seems to describe the degree of deformation resistance susceptibility to variation of hot-working condition, on the other hand, the remaining constant of these equations is deemed to effect on the intensity of flow stresses. However, in consideration that flow stresses are predicted to be zero at certain $\ln(Z/A)$ points, consequently, this type of equation appears to have a clear-cut limitation in predicting the intensity of flow stresses at a given Z value as anticipating the value of peak stress and steady stress might be impossible at the $\ln(Z/A)$ values below -9.83 and -8.17 respectively. Nevertheless, this linear form of relative equation would be beneficial to conclude the approximate intensity of flow stresses at hot-working condition range of the commercial production process.

3.2. DRXed grain size

Figure 4 shows the deformed microstructures of hot-extruded

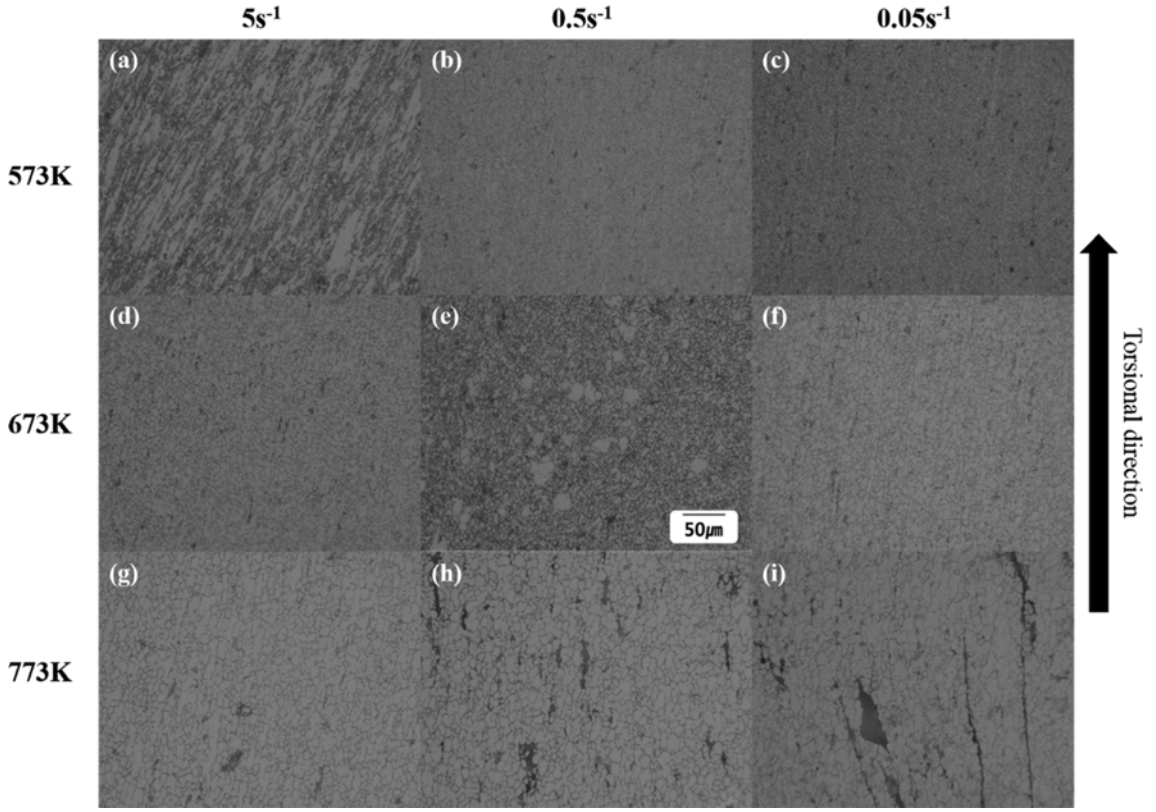

Fig. 4. Optical micrographs of deformed microstructure of fractured AA5083 after hot torsion test at (a), (b), (c) 573 K, (d), (e), (f) 673 K and (g), (h), (i) 773 K with strain rates of (a), (d), (g) 5 s^{-1}, (b), (e), (h) 0.5 s^{-1} and (c), (f), (i) 0.05 s^{-1}.

AA5083. D_{DRX} of AA5083 increased with decreasing strain rate and increasing temperature, namely, decreasing Z parameter value. The DRXed grain shape also displays notable differences with Z. DRX is an effective way to obtain a fine microstructure because it makes the large initial gain transform into a lot of smaller grains. As the mechanical properties of hot-worked materials are closely related with microstructures, especially grain size, the prediction of grain size corresponding to the deformation conditions would be useful for the metalworking industry. Previous studies reported that D_{DRX} does not depend on the initial grain size, but it could be expressed as a function of temperature and strain rate [9,16,17]. The empirical equation using dimensionless parameter, Z/A, can be established for the prediction of D_{DRX} with regard to deformation conditions. A linear regression of ln(Z/A) and ln(D_{DRX}) was derived from experimental data as presented in Fig. 5 and the equation of the fitted line is as follows:

$$D_{DRX} = 2.87(Z/A)^{-0.14}, \quad (7)$$

This equation predicts the DRXed grain size of hot-extruded AA5083 which corresponds to the Z parameter.

A tendency that the grains are of regular equiaxed shape for lower Z values, whilst as Z increases, the grains become larger and irregular (Fig. 4). These results are due to the strain hardening caused by the dislocation accumulation which

Table 2. Experimental parameters acquired from flow curve analysis

Deformation condition		ln(Z/A)	σ_p (MPa)	ε_p	σ_{ss} (MPa)	D_{DRX} (μm)
573 K	5 s^{-1}	8.27	211	0.73	150	1.05
	0.5 s^{-1}	5.97	198	0.47		1.06
	0.05 s^{-1}	3.67	158	0.32	122	1.28
673 K	5 s^{-1}	2.63	146	0.23	87	2.24
	0.5 s^{-1}	0.32	118	0.17		2.45
	0.05 s^{-1}	-1.98	91	0.06	62	4.17
773 K	5 s^{-1}	-1.56	100	0.10	48	3.97
	0.5 s^{-1}	-3.86	69	0.07		5.23
	0.05 s^{-1}	-6.16	48	0.04		6.15

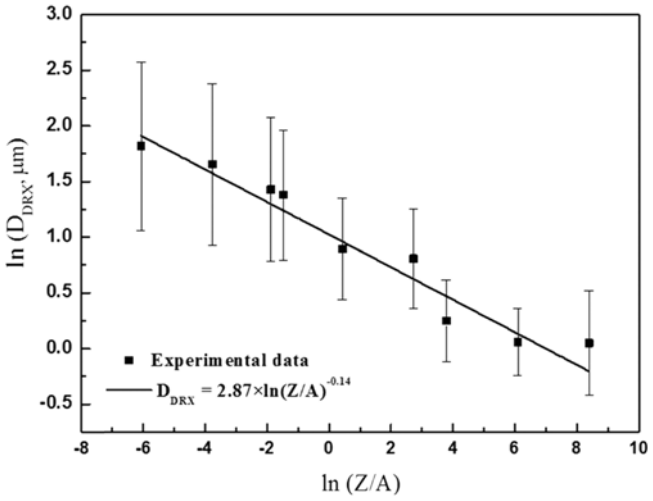

Fig. 5. Experimental data for D_{DRX} of hot-extruded AA5083 and a relationship between D_{DRX} and dimensionless parameter, Z/A.

appeared more active in higher Z condition, while restricted in lower Z values. Therefore, growth of the new recrystallized grains could be limited due to higher dislocation density on the grains at the condition of higher Z values and it leads to a reduction in the driving force for the grain growth, bringing about smaller D_{DRX}, consequently [18].

3.3. DRX fraction

It is generally accepted that solid transformation can be described by Avrami Eq. [19-21]. Avrami equation is available to imitate a dynamic solid transformation by the view that DRX is governed by the order of nucleation and growth processes, similar to static recrystallization. The Avrami equation for the kinetics of DRX with an exponential relationship of several mechanical parameters is shown as follows:

$$X_{DRX} = 1 - \exp\left\{-k\left(\frac{\varepsilon - \varepsilon_c}{\varepsilon^*}\right)^n\right\}, \quad (8)$$

where X_{DRX} is the volume fraction of DRXed grains, ε^* is the strain at the maximum strain softening rate, ε_c is the critical strain for the initiation of DRX, k and n are material constants.

Critical strain for the initiation of DRX, ε_c, is an important factor to describe DRX kinetics of a material and it can be calculated from the curve between work-hardening rate (WH rate) and flow stress as denoted in Fig. 6. Each curve presents a gradual decline in WH rate to zero, having a notable feature that the degree of decline is suppressed on a certain point of the curve. To be specific, the tendency of the decline is decelerated after a certain point of the curve due to formation of subgrains, obstructing the movement of dislocations, and it is eventually accelerated again by a decrease in dislocation density originated from initiating DRX process

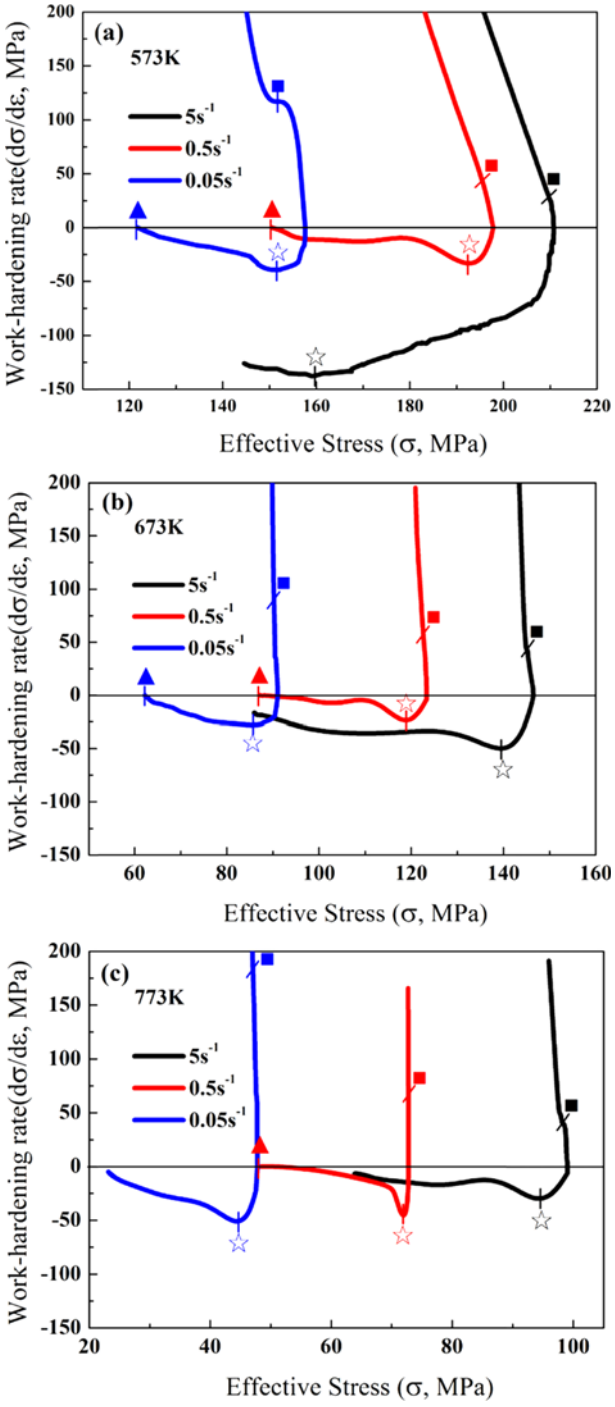

Fig. 6. Work hardening rate (=$d\sigma/d\varepsilon$)-effective stress (σ) curves of hot-extruded AA5083 at (a) 573 K, (b) 673 K and (c) 773 K. ■ = critical stress, ☆ = stress at minimum work-hardening rate, ▲= steady state stress.

[22]. Therefore, the inflection point of the curve where the decline tendency is reversed from deceleration to acceleration has to be the critical stress to initiate DRX process.

Figure 7 shows WH rate-effective stress curve of hot-extruded AA5083 deformed at 573 K with a strain rate of 0.05 s^{-1}. The curve denotes experimental parameters of peak

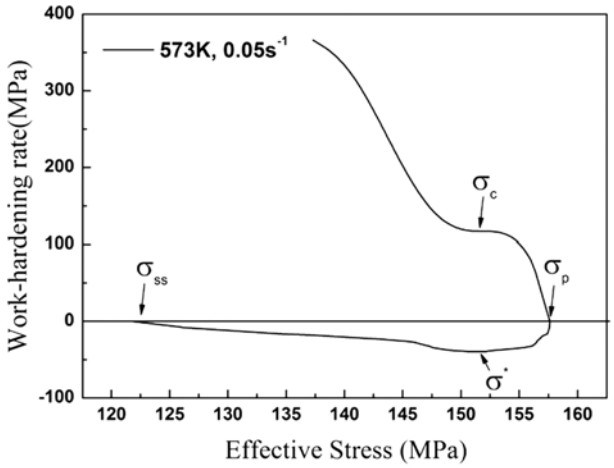

Fig. 7. WH rate-effective stress curve of hot-extruded AA5083 with the deformation condition of 573 K and 0.05 s^{-1} to determine the experimental parameters.

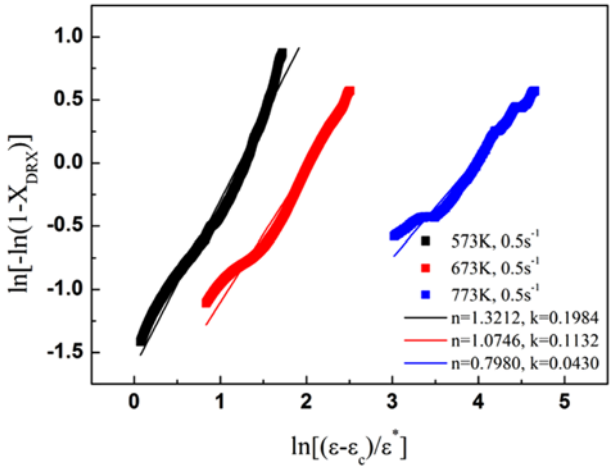

Fig. 8. A relationship between ln[-ln(1-X_{DRX})] and ln[(ε-ε_c)/ε^*] of hot-extruded AA5083 with a strain rate of 0.5 s^{-1} at various temperatures.

stress (σ_p), steady state stress (σ_{ss}), and the stress at a strain of minimum WH rate (σ^*). The acquired experimental parameters with various deformation conditions are listed in Table 3. These parameters were used for the following relationship to calculate X_{DRX} [23]:

$$X_{DRX} = \frac{\sigma - \sigma_p}{\sigma_{ss} - \sigma_p}, \quad (9)$$

The linear regression was used for the determination of material constants by combining Eq. (8) with Eq. (9). The linear relationship between ln[-ln(1–X_{DRX})] and ln[(ε–ε_c)/ε^*] determined the slope, n, and the intercept, ln$k$, as shown in Fig. 8.

The fraction of DRXed grains in hot-extruded AA5083 was measured by optical micrographs observation. Figure 9 indicates Avrami plots for X_{DRX} of AA5083 deformed at a strain rate of 0.5 s^{-1} at various temperatures, and the experimental data are also presented. However, large differences were found between Avrami plots and experimental data, and their differences were more significant at higher deformation temperature. Equation (9) is based on the idea that dynamic recrystallization is the dominating mechanism for the fall in flow stress during the hot working process and other factors dedicating to flow softening is assumed to be negligible.

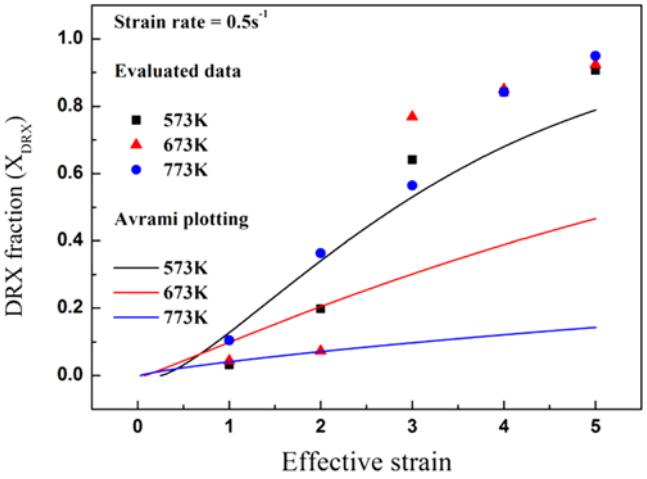

Fig. 9. Avrami plots and experimental data for hot-extruded AA5083 deformed with a strain rate of 0.5 s^{-1} at various temperatures.

According to several researches, however, the fall in flow stress at large strain has been ascribed to a various different mechanisms [24-27]. Except for dynamic recrystallization caused by decreasing dislocation density, reduction in the average Taylor factor or GBS can be considered attributing to the

Table 3. Experimental parameters acquired from flow stress - WH rate curve

Deformation condition		σ_c (MPa)	ε_c	σ^* (MPa)	ε^*
573 K	5 s^{-1}	178	0.42		
	0.5 s^{-1}	190	0.25	192.51	0.70
	0.05 s^{-1}	152	0.13	152.18	0.52
673 K	5 s^{-1}	145	0.12	139.55	0.64
	0.5 s^{-1}	123	0.08	118.90	0.40
	0.05 s^{-1}	91	0.04	85.36	0.24
773 K	5 s^{-1}	98	0.04	94.20	0.19
	0.5 s^{-1}	73	0.03	71.96	0.05
	0.05 s^{-1}	46	0.02	44.31	0.08

fall in flow stress during deformation. Therefore, a supplementary equation to Eq. (9) explaining the influence on the flow stress of other different mechanisms has to be figured out to establish the Avrami relationship for DRX in the case of this study.

To minimize the difference between theoretical value and experimental data, another attempt has been made in this study to apply another parameter to the Avrami relationship. Aside from the flow stress relationship, the change in micro-hardness with the variation of strain had been already reported as an applicable factor to derive Avrami equation from experimental result [28]. While the previous study was carried out with dissimilar constants to Eq. (9) such as hardness of cold-worked and homogenization to describe X_{DRX}, in this study, based on the phenomena that the micro-hardness of the experimental alloy gradually increases with increasing DRX fraction, it followed that analogous factors with Eq. (9) were more plausible to obtain Avrami equation. The modified model of Eq. (9) was acquired by substituting the flow stress to the micro-hardness as follows:

$$X_{DRX} = \frac{H - H_p}{H_{ss} - H_p}, \tag{10}$$

where H is the micro-hardness at a certain strain, H_p is the micro-hardness at a peak strain and H_{ss} is the micro-hardness at a steady state stress. In general, the mechanical properties have an inversely proportional relationship with the average grain size in the case of polycrystalline material, and thus, the hardness of a material generally increases as dynamic recrystallization is developed. Figure 10a shows a comparison between the observed DRX fraction and the micro-hardness data of hot-extruded AA5083 with the deformation condition of 573 K, 0.5 s^{-1}, and the values of those are not much different. However, the micro-hardness was dramatically fallen after certain strain at lower Z and strain rate conditions. For example, the hardness decreased from 96.5 Hv to 78.5 Hv at the strain of 2 and 3 at the deformation condition of 673 K, 0.5/s, respectively. It is considered that these results were originated from the activation of the cavity formation at lower Z and strain rate conditions as discussed in previous studies [29,30]. Higher strain rate condition of 5 s^{-1} was also not pertinent to Eq. (10) due to its difficulty in concluding the value of steady state stress hardness as shown in Fig. 6.

Figure 10b represents a linear regression for the determination of n and k at the deformation condition of 573 K, 0.5 s^{-1} by combining Eqs. (8) and Eq. (10). Acquiring Avrami constants by using Eq. (10) reveals a considerable difference compared with that by using Eq. (9); the value of n is 2.41 by the former, but 1.32 by the latter. A comparison between experimental data and Avrami plots at the given deformation condition is shown in Fig. 11. The Avrami relative equation for the given condition is identical to the following equation:

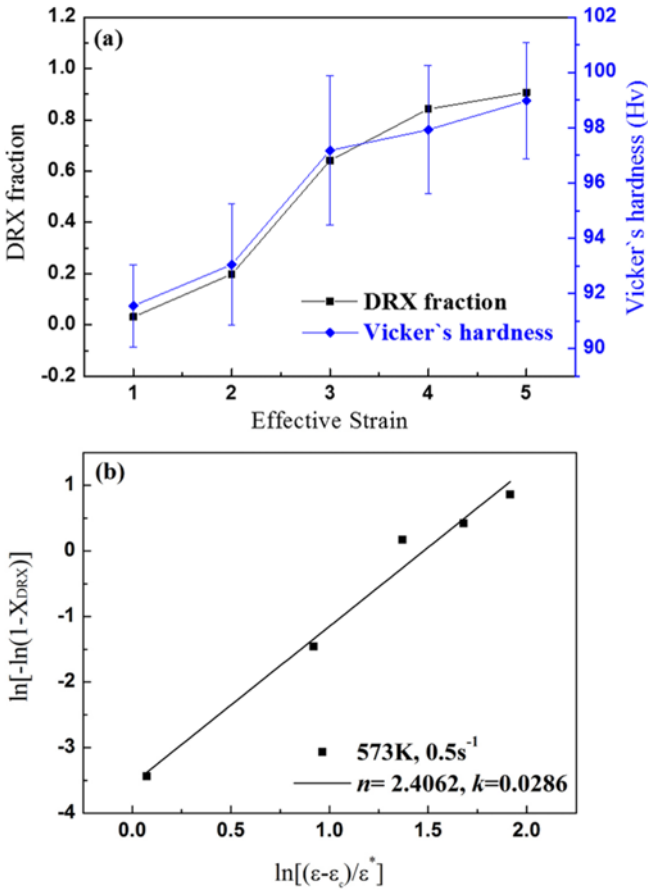

Fig. 10. Relationships between (a) X_{DRX} and micro-Vickers hardness at strains from 1 to 5 and between (b) ln[-ln(1-X_{DRX})] and ln[(ε-ε_c)/ε^*] of hot-extruded AA5083 at the deformation condition of 573 K, 0.5 s^{-1}.

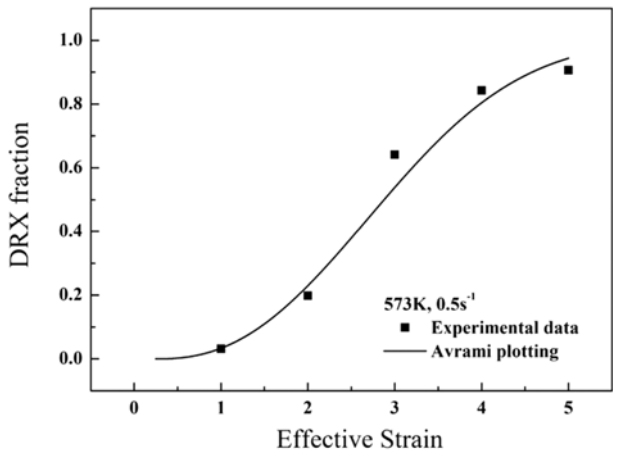

Fig. 11. A relationship between experimentally data and Avrami plot for X_{DRX} of hot-extruded AA5083 with the deformation condition of 573 K, 0.5 s^{-1}.

$$X_{DRX} = 1 - \exp\left\{-0.03\left(\frac{\varepsilon - 0.25}{0.70}\right)^{2.41}\right\}, \tag{11}$$

However, The Avrami model using the micro-hardness is seeming to have a severe drawback to apply for lower Z conditions. A supplementing model to Eq. (10) concerning Taylor factor variation and GBS will be studied to derive Avrami relationship in lower Z conditions.

4. CONCLUSIONS

DRX characteristics of hot-extruded AA5083 has been studied at various deformation conditions by using the hot torsion test, and the following conclusions are drawn:

(1) As the temperature increased and the strain rate decreased, the flow stress of hot-extruded AA5083 decreased but the ductility increased. The dependence of the peak and steady stresses on temperature and strain rate were established with dimensionless parameter Z/A.

$$\sigma_p = 11.84 \times \ln(Z/A) + 116.92$$

$$\sigma_{ss} = 10.46 \times \ln(Z/A) + 85.42$$

The above relationships confirmed that the softening mechanism of AA5083 was DRX.

(2) The DRXed grain size decreased with increasing Z conditions, and its dependence was expressed as follows:

$$D_{DRX} = 2.87(Z/A)^{-0.14}$$

(3) An empirical model using the micro-hardness is established in the form of the Avrami relationship as follows:

$$X_{DRX} = 1 - \exp\left\{-0.03\left(\frac{\varepsilon - 0.25}{0.70}\right)^{2.41}\right\}$$

The general type of prediction model using the fall in flow stress was not suitable on the experimental aluminum alloy. Reduction in the average Taylor factor and operation of GBS is regarded as the main reason for this effect.

ACKNOWLEDGEMENTS

This work was supported by Basic Science Research Program through the National Research Foundation of Korea (NRF) funded by the Ministry of Education (2016R1A6A3A11934765) and The Leading Human Resource Training Program of Regional Neo industry through the National Research Foundation of Korea (NRF) funded by the Ministry of Science, ICT and future Planning(2016H1D5A1910612).

REFERENCES

1. S. Malopheyev and R. Kaibyshev, *Mat. Sci. Eng. A* **620**, 246 (2014).
2. S. H. Hwang, H. M. Baek, H. S. Joo, and Y. T. Im, *Met. Mater. Int*. **21**, 391 (2015).
3. J. J. An, D. G. Lee, K. R. Lim, T. Y. Kim, Y. T. Lee, and S. Y. Yoon, *Korean J. Met. Mater.* **53**, 380 (2015).
4. J. W. Won, Y. M. Lee, J. T. Yeom, G. Y. Lee, and C. S. Lee, *Korean J. Met. Mater.* **54**, 338 (2016).
5. J. R. Cho, W. B. Bae, W. J. Hwang, and P. Hartley, *J. Mater. Process. Technol*. **118**, 356 (2001).
6. G. A. Henshall, M. E. Kassner, and H. J. McQueen, *Metall. Mater. Trans. A* **23**, 881 (1992).
7. T. Watanabe, *Mat. Sci. Eng. A* **166**, 11 (1993).
8. H. J. McQueen, E. Evangelista, J. Bowles, and G. Crawford, *Met. Sci.* **18**, 395 (1984).
9. W. Blum, Q. Zhu, R. Merkel, and H. J. McQueen, *Mat. Sci. Eng. A* **205**, 23 (1996).
10. T. Hirata, T. Osa, H. Hosokawa, and K. Higashi, *Mater. Trans.* **43**, 2385 (2002).
11. S. I. Kim and Y. C. Yoo, *Mat. Sci. Eng. A* **311**, 108 (2001).
12. S. I. Kim and Y. C. Yoo, *Met. Mater. Int.* **8**, 7 (2002).
13. M. Zhou and M. P. Clode, *Mater. Sci. Technol.* **13**, 818 (1997).
14. H. J. McQueen and N. Ryum, *Scand. J. Metall.* **14**, 183 (1985).
15. D. R. Barraclough, H. J. Whittaker, K. D. Nair, and C. M. Sellars, *J. Testing Eval.* **1**, 220 (1973).
16. S. H. Cho, Y. S. Kim, Y. C. Yoo, S. H. Rhim, and S. I. Oh, *Korean J. Met. Mater.* **36**, 502 (1998).
17. T. Sakai and J. J. Jonas, *Acta. metall.* **32**, 189 (1984).
18. A. I. Fernandez, P. Uranga, and B. Lopez, *Mat. Sci. Eng. A* **361**, 367 (2003).
19. M. Avrami, *J. Chem. Phys.* **7**, 1103 (1939).
20. M. Avrami, *J. Chem. Phys.* **8**, 212 (1940).
21. W. A. Johnson and R. F. Mehl, *Trans. Am. Inst. Min. Engrs.* **135**, 396 (1939).
22. E. I. Poliak and J. J. Jonas, *Acta. Mater.* **44**, 127 (1996).
23. J. Liu, Z. Cui, and L. Ruan, *Mat. Sci. Eng. A* **529**, 300 (2011).
24. H. J. McQueen, J. K. Solberg, N. Ryum, and E. Nes, *Philos. Mag. A* **60**, 473 (1989).
25. H. J. McQueen, O. Knustad, N. Ryum, and J. K. Solberg, *Scripta Metall.* **19**, 73 (1985).
26. G. R. Canova, U. F. Kocks, and J. J. Jonas, *Acta Metall.* **32**, 211 (1984).
27. T. Pettersen and E. Nes, *Metall. Mater. Trans. A* **34**, 2727 (2003).
28. S. Mandal and P. V. Sivaprasad, *J. Mater. Sci*. **42**, 2724 (2007).
29. D. H. Bae and A. K. Ghosh, *Acta. Metall.* **50**, 993 (2002).
30. D. H. Bae and A. K. Ghosh, *Acta. Metall.* **50**, 1011 (2002).